Composite dielectric metasurfaces for phase control of vector field

Sung W. Kim,[1,*] Ki Ju Yee,[2] Maxim Abashin,[3] Lin Pang,[3] and Yeshaiahu Fainman[3]

[1]*Materials Science and Engineering, University of California San Diego, 9500 Gilman Drive, La Jolla, California 92093, USA*

[2]*Department of Physics, Chungnam National University, Daejeon 305-764, South Korea*

[3]*Department of Electrical and Computer Engineering, University of California San Diego, 9500 Gilman Drive, La Jolla, California 92093, USA*

**Corresponding author: swk018@ucsd.edu*

Received March 9, 2015; revised May 1, 2015; accepted May 5, 2015;
posted May 5, 2015 (Doc. ID 235808); published May 19, 2015

We designed, fabricated, and characterized a dielectric metamaterial lens created by varying the density of subwavelength low refractive index nanoholes in a high refractive index substrate, resulting in a locally variable effective refraction index. It is shown that a constructed graded index lens can overcome diffraction effects even when the aperture/wavelength (D/λ) ratio is smaller than 40. In addition to the conventional design of a polarization insensitive lens, we also show that a polarization diversity lens ($f_o \neq f_e$) can be realized by arranging nanoholes in patterns with variable density in different transverse directions. Such a anisotropic microlens demonstrates polarization dependent focal lengths of 32 and 22 μm for linearly x- and y-polarized light, respectively, operating at a wavelength of $\lambda = 1550$ nm. We also show numerically and demonstrate experimentally achromatic performance of the devices operating in the wavelength range of 1500–1900 nm with full width at half-maximum (FWHM) of the focal spots of about 4 μm.

OCIS codes: (050.1970) Diffractive optics; (050.1965) Diffractive lenses; (050.6624) Subwavelength structures.
http://dx.doi.org/10.1364/OL.40.002453

Diffractive optical elements are among the most commonly used compact components in applications involving the manipulation of quasi-monochromatic light, including optical systems for beam shaping, deflecting, collimating, and imaging, as well as for displays. Diffractive optical elements [1–6] have been developed for visible to near infrared wavelengths to replace bulky optical components by compact planar elements. However, such elements can only be designed for monochromatic light and, furthermore, involve complex surface profiles that are difficult to fabricate. Moreover, these approaches require a minimum aperture size to avoid aperture-limiting diffraction affecting focusing power of the lens and causing aberrations. For example, prior reports show that, when the aperture/wavelength (D/λ) is smaller than 40, diffraction dominates the refractive effects [7].

To overcome these issues, a number of nanoscale engineered surface approaches have been investigated. Planar binary surfaces with subwavelength patterns have been developed in the past [8–14] and, by using a plasmonic surface, phase modulation of the transmitted wave was achieved [15]. However, plasmonic surfaces are impractical for transmission optics applications because such plasmonic metasurfaces result in very low transmission because of strong intrinsic absorption within the operating spectral bandwidth. For practical transmission optics applications, dielectric subwavelength nanostructures have been proposed for realization of a variety of optical components. One such component is a metasurface lens using nanopillars on an Si substrate for operation at a wavelength of 1550 nm and on an oxide substrate for operation in visible spectral range [16,17]. Dielectric grating reflectors with focusing effect were proposed using nonperiodic patterning of the grating surface [18]. Ultrathin gratings, lenses, and axicons have been reported, exploiting the patterning of a 100 nm thick Si layer into a dense arrangement of Si nanoantennas [19].

In this Letter, we explore the design parameters for engineering the effective refractive index of a composite dielectric created by controlling the density of deeply subwavelength low index nanoholes (e.g., air) in a high index dielectric layer (e.g., Si). The phase of the optical wavefront incident on such a composite dielectric is modulated by the local effective index of the layer. Intuitively, when an Si layer is perforated by a high density of air nanoholes, the composite layer will possess a low effective index close to that of air. Alternatively, when the density of air nanoholes is low, the effective index of the composite layer will be close to that of Si. Such planar layer composite dielectrics enable full space-variant control of the optical wavefront phase and allow for the realization of graded index lenses with polarization dependent focal length and graded index beam phase plates.

The distance between the nanoholes must be deeply subwavelength to avoid diffraction effects and, therefore, support only near field evanescent modes. Thus, the distance between the nanoholes should be less than λ_0/n, where λ_0 is the wavelength of incident light in a vacuum and n is the refractive index of the host medium layer (e.g., that of bulk Si). For example, for the Si nanostructure designed for operation with an incident light wavelength of 1550 nm, the distance between the nanoholes can be varied from 150 to 400 nm to achieve a low and high effective refractive index, respectively. The depth h, the thickness of the composite dielectric, is chosen to be about ~600 nm avoid 2π phase wrapping, resulting in the phase mask depth variation, $\Delta\phi \sim 2\pi\delta n(h/\lambda_0) < 2\pi$. Figure 1(a) shows the calculated effective refractive index for nanoholes with fixed diameters of 50 nm (red curve) and 100 nm (blue curve) versus the distance between the nanoholes. These calculations are based on the volume average theory [20,21], showing that the effective refractive indices are proportional to

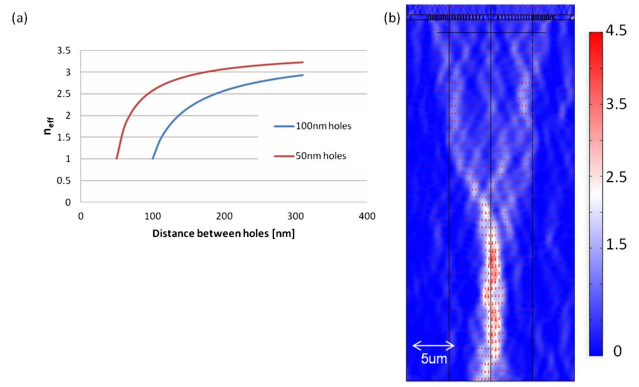

Fig. 1. (a) Effective index of an Si-based ($n_s = 3.5$) composite dielectric layer versus density of perforating lattice of air nanoholes with diameters of 50 (red curve) and 100 nm (blue curve). (b) COMSOL (FEM) simulations (two-dimensional) of power distribution of transmitted plane wave through the dielectric composite lens at 1550 nm wavelength for design A, where the color scale is normalized by the incident field intensity ($I_{\text{output}}/I_{\text{input}}$) showing the focusing effect.

volumetric fill factor and can be varied between 1.5 and 3. By varying the density of nanoholes in various regions of the composite dielectric slab, an arbitrary refractive index distribution can be achieved and used for lossless, space variant isotropic and anisotropic phase modulation of the transmitted optical field.

To demonstrate the concept, we have developed two designs for ultrathin dielectric microlenses with space invariant and space variant nanohole distributions, to implement polarization independent and polarization dependent impulse response designs, respectively. A polarization independent graded index (GRIN) microlens employs a locally symmetric square lattice of nanoholes, with local spacing $\Delta_x = \Delta_y$, whereas a polarization dependent GRIN microlens employs a locally asymmetric rectangular lattice of nanoholes, with local spacing $\Delta_x \neq \Delta_y$. The lattice spacing for each design varies according to a smooth radial dependence of the local phase profile on transmission.

These lenses are designed to consist of concentric regions, where each region is formed by a discrete collection of square or rectangular unit cells perforated by nanoholes for isotropic and anisotropic effective index modulation, respectively. While an individual hole radius is kept constant over the entire lens surface, the hole density is different in each region. For example, the region in the center of the lens is about a 2×2 μm square area and is perforated by a low density nanohole array; the region at the edge of the lens is about 1.15×1.15 μm squares and is perforated by high density nanoholes. The regions at the lens edge are designed with a smoother graded index profile based on smaller unit cells, with a fine density variation. Consequently, the nanohole periodicity changes from region to region. We performed computer simulations for propagation of an incident plane wave through such a composite dielectric slab lens using COMSOL Multiphysics (FEM, Finite Element Method). The intensity distribution of the transmitted light is shown in Fig. 1(b), demonstrating the focusing effect.

For experimental validation, we explored two lens designs: a polarization independent graded index lens by symmetric design (design A. $\Delta_x = \Delta_y$) and a polarization dependent graded index lens by asymmetric design (design B. $\Delta_x \neq \Delta_y$). For design A, the spacing in between the nanoholes starts from 150 nm near the edge of the substrate and increases to 400 nm at the center with 50 nm increments for each spacing. For design B, the spacing ranges from 200 to 400 nm with 100 nm increments.

The composite dielectric nanostructures were fabricated by patterning Ni circular holes in the designed patch configuration as a mask for dry etching of a 0.5 m thick Si substrate. The process consists of electron beam lithography and liftoff processing to fabricate the designed Ni-mask. Ninety nm thick PMMA and 90 nm HSQ layers were spin coated onto a double-side polished silicon substrate. The nanohole regions of our design were first patterned into the PMMA layer by a Vistek EBPG 5200 electron beam writer. After lithography, HSQ resist and PMMA were developed, and a 40 nm Ni layer was deposited via electron beam evaporation to create a mask for consequent dry etching. The PMMA resist was then removed via liftoff, leaving the Ni mask with nanohole patterns on the substrate. Si substrate was etched using plasma etching to a depth of about 570 nm, followed by Ni mask removal using a wet Ni etchant. The SEM image of the fabricated lens (design B) is shown in Fig. 2(a), demonstrating that fabricated regions are perforated by low and high density nanoholes in the center and at the edges of the lens (graded with fill factor of 1 to 0). Figures 2(c) and 2(d) show a zoom in nanostructure for symmetric and asymmetric nanohole lattice arrangements, respectively (e.g., in symmetric design $\Delta_x = \Delta_y$, in asymmetric design $\Delta_x \neq \Delta_y$). For asymmetric design, the graded effective indices in the x direction (i.e., Δn_{eff_x}) and the y direction (Δn_{eff_y}) are different and are expected to impose different impulse responses for the linearly polarized optical field in these two orthogonal directions. Consequently, modulation of the light wavefront phase passing through the composite dielectric structure is determined by the polarization

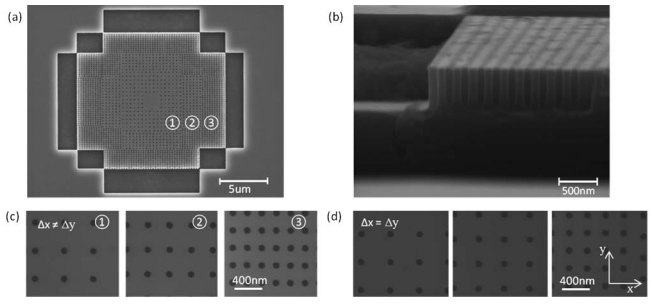

Fig. 2. SEM images of fabricated structures: (a) top view of the fabricated lens with asymmetric design B; (b) side view image of the dielectric composite lens with estimated depth of about 570 nm; (c) rectangular lattices of nanoholes used in asymmetric design B for the corresponding lattices of nanoholes in ①, ②, and ③ regions: 400×400 nm, 350×300 nm and 250×200 nm; and (d) square lattices of perforating nanoholes for symmetric design A in regions 400×400 nm, 300×300 nm, and 250×250 nm.

of incident light. The etched nanohole depth reaches about 570 nm, as shown in Fig. 2(b) (i.e., side-view SEM image of fabricated lens, design B).

To experimentally validate the focusing effect of the composite dielectric microlens, a linearly polarized 1550 nm laser beam was demagnified to assure plane wavefront illumination of the fabricated devices. The spatial distribution of a beam, transmitted through the element, was imaged onto a CCD camera (XEVA-CL-320, 320×256 pixels with a 30 μm pixel pitch). By scanning the imaging lens along the optical axis, the evolution of the beam distribution along the optical axis was captured at each scan position. Figure 3 shows intensity distribution at the measured focal point behind the composite dielectric lens with a total efficiency about 50%. The efficiency can be improved further by depositing anti-reflection (AR) coatings on the high refractive index substrate. For the symmetric design A, the light is focused with highest intensity at a distance of about 35 μm behind the composite dielectric lens. The focusing occurs at the same plane for both x- and y-polarized incident beams. As expected, however, for our asymmetric design B, the measured focal length for x-polarized incident light decreased to 22 μm because of the large difference in the nanohole density in the x direction (Δ_x). For the y-polarized light, the performance is similar to that of the symmetric design.

The intensity distribution in the focal plane of the lens is shown in Fig. 3(c) for symmetric design A, and in Fig. 3(d) for asymmetric design B. The full width at half-maximum (FWHM) of both focal spots are about 4 μm, which is much smaller than the patterned lens aperture (i.e., a diameter of 20 μm). From the estimated focal length of 35 μm and diameter of 20 μm for a wavelength of 1550 nm, we expect a focal spot size of about 5 μm diameter (using expression $2\lambda f/D$ with focal length f

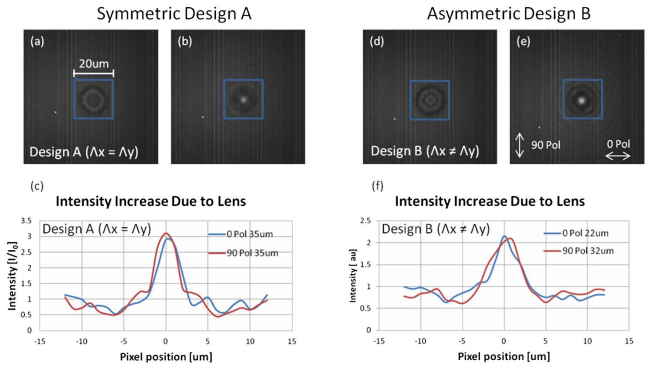

Fig. 3. Measured light intensity distribution of fabricated composite dielectric slab lens. Captured images (a) and (d) show the intensity distribution at the lens surface, whereas (b) and (e) are images captured in the focal plane of the composite dielectric lens. The lens aperture is defined by the blue box. As expected, the focal spot size in (b) and (d) are much smaller than the lens aperture. (c) The measured intensity distribution for symmetric design A provides a focal length of $f = 32$ μm for both x-and y-linearly polarized incident fields. (f) For the asymmetric designs B, the estimated focal length remains the same (i.e., 32 μm) for the y-polarized incident field, but for the x-polarized field the focal length decreases to $f = 22$ μm. The intensity scale in (c) and (f) are $I_{\text{output}}/I_{\text{input}}$.

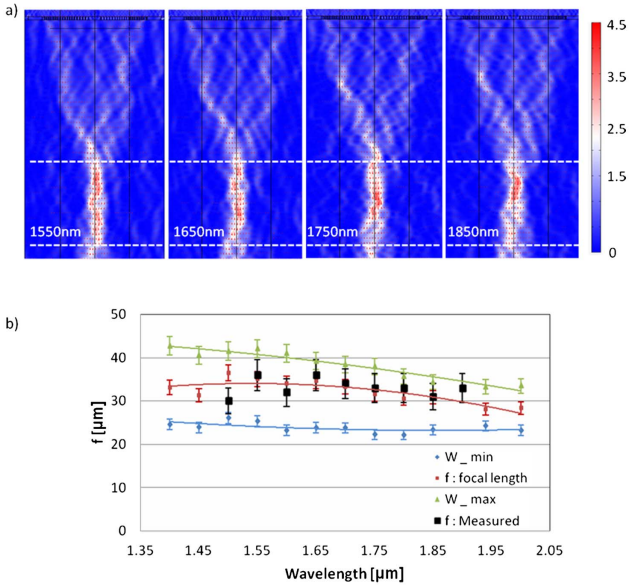

Fig. 4. (a) COMSOL (FEM) simulation of light intensity distribution at the operating wavelengths of 1550 1650, 1750, and 1850 nm shows similar performance; (b) COMSOL (FEM) simulation of focal length; f (red dots) and focal depth; w, spot length of $I_{\text{output}}/I_{\text{input}} \geq 2.0$ (blue to green lines) for the composite dielectric lens operating in the wavelength range 1400–2000 nm and measured focal length; f results (black square). The change in focal length (red dot) is smaller than that of the depth of focus.

and aperture of the lens D, $\text{NA} = n \cdot \sin\theta \sim \frac{nD}{2f} \sim 0.3$), which is in good agreement with our measured result. This result shows that with our approach it is possible to overcome diffraction effects even when aperture/wavelength (D/λ) is smaller than 40 [7]. Moreover, our approach may enable realization of composite dielectric lens with further improved performance through design of the effective refractive index varied as higher order phase polynomials.

Finally, it should be noted that a composite dielectric lens allows for continuous control of the phase profile (from 0 to 2π) and may enable unique functionalities with little to no dependence on the wavelength of operation. To validate this hypothesis, we investigate the element response for broad spectral range operation. The FEM computer simulations of the intensity distribution for light transmitted through the composite dielectric lens show nearly constant focal length at the wavelengths of 1550, 1650, 1750, and 1850 nm sampling points, demonstrating the robustness of the lens as a broadband element. We also conducted calculations and compared to experiments to validate the broad band operation of the fabricated element. The calculations and the experimental results of focal length and focal depth, w (spot length of $I_{\text{output}}/I_{\text{input}} \geq 2.0$) in wavelength range from 1450 to 2000 nm are shown in Fig. 4(b). The change in focal length is smaller than that of the depth of focus (about 25 to 40 μm) over all wavelengths. This fact suggests that our element can act as a broadband achromatic microlens.

In conclusion, we have demonstrated a thin planar composite dielectric nanosurface lens patterned with subwavelength, space variant nanoholes on a silicon

wafer surface. The microlenses can be made polarization dependent by asymmetric design, as well as polarization independent by symmetric design operating with radiation from a broad spectral range. The main advantages of our dielectric nanosurface lenses include further reduction of insertion loss by adding AR coating and of element size and weight via submicron thickness fabrication and miniaturization. Such advantages make our structure readily suitable for a variety of applications, such as microlens arrays, high resolution CCD sensors, and other miniature imaging systems. The experimental results demonstrate the practical potential of polarization and/or position dependent graded index components by asymmetric designs. We envision using Cartesian and/or polar coordinate designs for future nanohole region realizations, such as space variant circular nanohole patterns or space invariant elliptical nanohole patterns. In addition, we plan to develop scalable composite dielectric nanosurfaces with higher order polynomial designs to achieve exceptional focusing power and overcome diffraction effects.

This work was supported by the Office of Naval Research Multi-Disciplinary Research Initiative, the National Science Foundation (NSF), the NSF Center for Integrated Access Networks, the Defense Advanced Research Projects Agency SCENICC Program under contract W911NF-11-C-0210, and the Cymer Corporation.

References

1. L. d'Auria, J. P. Huignard, A. M. Roy, and E. Spitz, Opt. Commun. **5**, 232 (1972).
2. H. Haidner, J. T. Sheridan, and N. Streibl, Appl. Opt. **32**, 4276 (1993).
3. B. Goebel, L. L. Wang, and T. Tschudi, Appl. Opt. **35**, 4490 (1996).
4. J. N. Mait, D. W. Prather, and M. S. Mirotznik, J. Opt. Soc. Am. A. **16**, 1157 (1999).
5. F. Fujita, H. Nishihara, and J. Koyama, Opt. Lett. **7**, 578 (1982).
6. P. Kipfer, M. Collischon, H. Haidner, and J. Schwider, Opt. Eng. **35**, 726 (1996).
7. M. A. Alvarez-Cabanillas, F. Xu, and Y. Fainman, App. Opt. **43**, 2242 (2004).
8. P. Lalanne, S. Astilean, P. Chavel, E. Cambril, and H. Launois, J. Opt. Soc. Am. A **16**, 1143 (1999).
9. M. S. Lee, P. Lalanne, J. C. Rodier, and E. Cambril, Opt. Lett. **25**, 1690 (2000).
10. E. Hasman, V. Kleiner, G. Biener, and A. Niv, App. Phy. Lett. **82**, 328 (2003).
11. S. Vo, D. Fattal, W. V. Sorin, Z. Peng, T. Tran, M. Fiorentino, and R. G. Beausoleil, IEEE Photon. Technol. Lett. **26**, 1375 (2014).
12. U. Levy, M. Nezhad, H. C. Kim, C. H. Tsai, L. Pang, and Y. Fainman, J. Opt. Soc. Am. A **22**, 724 (2005).
13. U. Levy, M. Abashin, K. Ikeda, A. Krishnamoorthy, J. Cunningham, and Y. Fainman, Phys. Rev. Lett. **98**, 243901 (2007).
14. F. Lu, F. G. Sedgwick, V. Karagodsky, C. Chase, and C. J. Chang-Hasnain, Opt. Express **18**, 119 (2007).
15. N. Yu and F. Capasso, Nat. Mater. **13**, 139 (2014).
16. P. R. West, J. L. Stewart, A. V. Kildishev, V. M. Shalaev, V. V. Shkunov, F. Strohkendl, Y. A. Zakharenkov, R. K. Dodds, and R. Byren, Opt. Express **22**, 26212 (2014).
17. D. Fattal, J. Li, Z. Peng, M. Fiorentino, and R. G. Beausoleil, *Advanced Photonics*, OSA Technical Digest (CD) (Optical Society of America, 2011), paper ITuD2
18. D. Fattal, J. Li, Z. Peng, M. Fiorentino, and R. G. Beausoleil, Nat. Photonics Lett. **4**, 466 (2010).
19. D. Lin, P. Fan, E. Hasman, and M. L. Brongersma, Science **345**, 298 (2014).
20. M. M. Braun and L. Pilon, Thin Solid Films **496**, 505 (2006).
21. J. A. del Rio and S. Whitaker, Trans. Por. Med. **39**, 159 (2000).